Using computer modeling analysis in single junction *a*-SiGe:H *p–i–n* solar cells

F. A. Rubinelli
INTEC, Universidad Nacional del Litoral, Güemes 3450, 3000 Santa Fe, Argentina

R. Jiménez, J. K. Rath,[a] and R. E. I. Schropp
Debye Institute, Utrecht University, P.O. Box 80000, NL-3508 TA Utrecht, The Netherlands

(Received 12 March 2001; accepted for publication 26 November 2001)

In this article we discuss basic aspects of single junction *a*-SiGe:H $p-i-n$ solar cells by coupling computer simulations with experimental characteristics. We are able to fit the dark illuminated current–voltage characteristics and the spectral response curves of *a*-SiGe:H $p-i-n$ structures in the initial state, modeling the density of dangling bonds in each device layer by using either uniform density profiles or the defect pool model. Although we can fit these experimental curves with any of these two electrical models, band gap profiling in the *a*-SiGe:H intrinsic layer leads to improvement of the solar cell performance only when the defect pool model is implemented in our simulations. A U-shaped band gap profile is tailored in our samples by a staircase band gap profile composed of (i) several front band gap graded steps, (ii) one lowest band gap region, and (iii) several back band gap graded steps. Only by using the defect pool model are we able to predict an optimum thickness for the front band gap graded steps and for a buffer layer located at the p/i interface. Furthermore, using the defect pool model, the simulation predicts that higher efficiencies in single junction *a*-SiGe:H $p-i-n$ solar cells can be achieved by depositing nonuniform graded steps, i.e., thicker band gap graded layers besides the lowest band gap *a*-SiGe:H layer and thinner band gap graded layers besides the p/i and i/n interfaces. © *2002 American Institute of Physics.* [DOI: 10.1063/1.1435416]

I. INTRODUCTION

Hydrogenated amorphous silicon germanium (*a*-SiGe:H) has proved to be a suitable low band gap material for the intrinsic layer in the bottom subcell of a tandem solar cell structure.[1] The main advantage of *a*-SiGe:H is that by controlled incorporation of germanium the optical band can be tuned within a wide energy range to values lower than those found in hydrogenated amorphous silicon (*a*-Si:H). However, lower optical band gaps are accompanied by significant deterioration of the electronic properties. Alloying of *a*-Si:H with Ge increases the Urbach tail and the dangling bond density. In order to reduce the impact of these undesired properties of *a*-SiGe:H based solar cells a profiled band gap is utilized in the intrinsic layer.[2] The art of designing the optimum profile for the conduction and for the valence band edges is usually known as band gap engineering. It was shown in the literature that the band gap profile implemented in the intrinsic layer of *a*-SiGe:H $p-i-n$ solar cells has a strong influence on the open circuit voltage (V_{oc}) and fill factor (FF).[2] Usually an asymmetrical U- or V-shaped distribution is implemented in these cells for the band gap of its intrinsic layer. In other words, the band gap of the whole intrinsic layer or part of it is linearly graded and the band gap minimum is placed closer to the p/i interface than to the i/n interface. The dependence of current–voltage ($J-V$) characteristics under dark and illumination conditions and the spectral response (SR) with respect to the position of the band gap minimum in V-shaped profiles were studied experimentally and numerically.[3] Alternative designs were also proposed in the literature for the intrinsic *a*-SiGe:H band gap in order to optimize the solar cell performance like, for instance, double U-shaped and W-shaped profiles.[4] Band gap profiles are obtained, in practice, by depositing several thin layers of different optical gaps and material properties that do not change with depth (in this article we will call these layers band gap graded layers). In our samples this is the case in which the U-shaped band gap profile is implemented by a staircase type band gap profile. Charged defects present in these band gap graded layers screen the electric field created by ionized impurities of both doped layers, and strongly influence the extraction of photogenerated carriers. Because of the complexity of the *a*-SiGe:H $p-i-n$ structure it is quite attractive to use computer simulations to gain more insight into the electrical transport taking place inside the cell and to explore alternative band gap grading techniques for further optimization of the solar cell performance. This effort has to be accompanied by the use of self-consistent input parameters and updated device modeling, avoiding any misleading answer.

In this article, we will show that for *a*-SiGe:H single junction solar cells in the annealed state, fitting of experimental data can be performed by adopting two different density of dangling bond (DB) representations: uniform (constant) density of the DB in every device layer and the defect pool model. However these two alternative DB representa-

[a]Corresponding author; electronic mail: j.k.rath@phys.uu.nl

tions could lead to quite dissimilar computer modeling predictions. We will show that when the density of DBs is assumed to be constant in each device layer our computer program is not able to help us in designing the optimum band gap profile for the *a*-SiGe:H intrinsic layer. On the other hand, when the defect pool model is implemented in our code we are able to justify the presence of band gap profiles in the intrinsic layer and our predictions are in agreement with experimental evidence. In this study we will focus our attention on the application of *a*-SiGe:H $p-i-n$ structures as bottom cells of *a*-SiGe:H/*a*-SiGe:H tandem solar cells.

II. EXPERIMENTS

Single junction $p-i-n$ solar cells with *a*-SiGe:H *i* layer were grown by plasma enhanced chemical vapor deposition (PECVD) in an ultrahigh vacuum multichamber system (PASTA). Cells were deposited onto SnO_2 coated glass (Asahi U type) in the superstrate configuration, SnO_2/*p*-*a*-SiC:H/*i*-*a*-SiGe:H U-shape/*n*-*a*-Si:H/Ag. Thin buffer layers of *a*-Si:H were included between the *p*- and *n*-doped layers and the intrinsic layer. A linear asymmetrical U-shape band gap profile was implemented in the *a*-SiGe:H intrinsic layer by varying the Ge content in the film. In the particular solar cell under analysis in this article a staircase profile of four steps between buffer layers and the lowest band gap layer ($E_g \sim 1.53$ eV) was implemented. The absorption coefficient and refractive indices of each individual *a*-SiGe:H layer were determined by reflection/transmission (R/T) measurements. The total density of the dangling bond and the Urbach tail were extracted with the constant photocurrent method (CPM) technique. The activation energy of each single layer was obtained from the temperature dependence of the dark conductivity extracted with a Keithley 617 electrometer (after annealing at 160 °C for 1 h inside a vacuum chamber). Single junction *a*-SiGe:H $p-i-n$ solar cells were characterized by their dark $J-V$ characteristics, light $J-V$ with AM1.5 illumination, and spectral response (SR) measurements.

To be specific, the solar cell that we investigate in this article has the following structure: glass/SnO_2/*p*-*a*-SiC:H/buffer (*a*-Si:H, 1.80 eV, 6 nm)/four grading steps (2 nm each, 8 nm total)/*i*-*a*-SiGe:H (1.53 eV, 80 nm)/four grading steps (10 nm each, 40 nm total)/buffer (*a*-Si:H, 1.8 eV, 8 nm)/*n*-*a*-Si:H/Ag. This structure presents a short circuit current (J_{sc}) of 18.8 mA/cm^2, an open circuit voltage (V_{oc}) of 0.7 V, a fill factor of 0.58, and an efficiency (η) of 7.63% in the initial state.

III. MODELING

A. General considerations and input parameters

Our simulations were performed with the computer code D-AMPS where D-AMPS stands for AMPS' core (analysis of microelectronic and photonic devices developed at The Pennsylvania State University, University Park, PA[5]) plus some new developments. These new developments refer to the inclusion in AMPS of amphoteric states,[6] the defect pool model,[7,8] and scattering at rough surfaces.[9] In this article we model the density of dangling bonds using two different

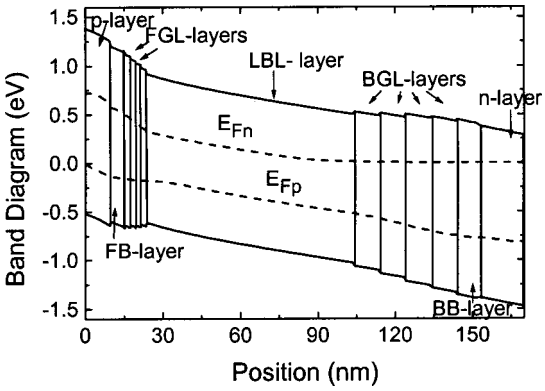

FIG. 1. Computer generated band diagram of the *a*-SiGe:H $p-i-n$ solar cell at short circuit conditions. The light source is AM1.5. The quasi-Fermi levels for electrons (E_{Fn}) and holes (E_{Fp}) are shown by the dotted lines.

electrical approaches: (a) The uniform density model (UDM) of gap states in each device layer and (b) the defect pool model (DPM) proposed by Powell and Deane.[7,8] The density of states in the UDM model is described by three different Gaussian distributions, D^-, D^0, and D^+. The peak energies of these Gaussians are located in the lower half of the band gap (D^-), close to the Fermi level of the intrinsic material (D^0), and in the upper half of the band gap (D^+), respectively. The ratio of charged to neutral defects adopted was 4:1 in the *a*-Si:H buffer and doped layers,[7] 6:1 in the *a*-SiGe:H lowest band gap intrinsic layer,[4] and equal to ratios between 4:1 and 6:1 in band gap graded layers. The correlation energy U was assumed equal to 0.2 eV in every layer. The peaks of the Gaussians were spaced 0.3 eV apart in energy along the entire device. The separation between the nonoccupied D^+ peak and the double occupied D^- peak, usually known as Δ, was therefore adopted to equal 0.4 eV and was independent of the band gap. In the DPM approach the total hydrogen concentration H was assumed to be 5×10^{21} cm^{-3}, the correlation energy was fixed to 0.2 eV, and the freezing temperature was equal to 500 K. The most probable energy E_P in the distribution of available states was used as a ''pseudofree'' fitting input parameter and the pool width was appropriately selected to reproduce the same value of $\Delta = 0.4$ eV in each layer. Of the three different microscopic chemical reactions proposed by Powell and Deane we selected the reaction in which only one Si–H bond is broken and the hydrogen atom diffuses to the weak-bond site, breaking the weak bond.[10] The other two alternative mechanisms give rise to either too low or too high a density of DBS in the materials under analysis.

In the *a*-SiGe:H $p-i-n$ structure under study we will call the buffer layers located at the p/i and i/n interfaces front buffer (FB) and back buffer (BB) layers, respectively. The four grading steps or layers that define the staircase band gap profile between the buffer (FB and BB) layers and the lowest band gap layer (LBL) will be termed the front and the back band gap graded layer (FGL and BGL, respectively). Finally, LBL will represent the region where the U-shaped band gap of *a*-SiGe:H bears its minimum. Figure 1 illustrates our nomenclature, showing the band diagram of the $p-i-n$

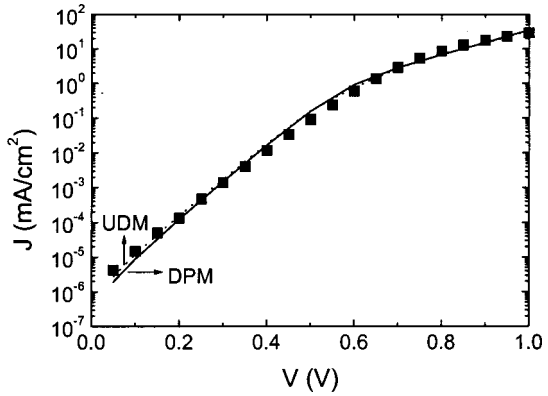

FIG. 2. Measured (square symbols) and simulated dark current–voltage characteristics of the single *a*-SiGe:H $p-i-n$ solar cell. UDM (dotted lines) and DPM (solid lines).

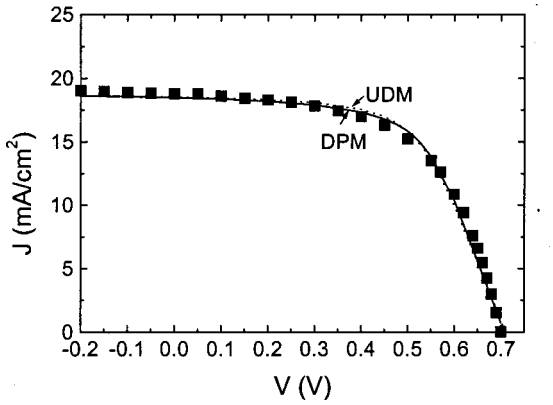

FIG. 3. Measured (square symbols) and simulated illuminated current–voltage characteristics of the single *a*-SiGe:H $p-i-n$ solar cell. UDM (dotted lines) and DPM (solid lines).

a-SiGe:H at short circuit conditions predicted by D-AMPS under AM1.5 illumination.

The activation energies of both doped layers were derived from dark conductivity measurements taking into account the Fermi level shifts when we move from 0 K to room temperature. Our resulting values were 0.47 and 0.24 eV for *p*-*a*-SiC:H and *n*-*a*-Si:H layers, respectively. The electrical parameters that cannot be directly measured were adopted as equal to standard values found in the literature or those from the best fits of our experimental curves. For instance, in the *a*-SiGe:H and *a*-Si:H layers the electron and hole mobilities adopted were 20 and 2 $cm^2/V\,s$, respectively, and these values were lower by a factor of 2 in *a*-SiC:H. In all the device layers, the effective densities of states N_c and N_v were assumed to be $2\times10^{20}\ cm^{-3}$ and the cross sections were 5×10^{-15} and $5\times10^{-16}\ cm^2$ for charged and neutral states, respectively, in both the tails and midgap states. Since there is not yet a clear picture available of the distribution of energy offsets at each interface of the various layers present in this cell structure, we decided to split the band gap offsets equally between the conduction and the valence bands. The total density of dangling bonds and the slope of the valence band tail in the LBL *a*-SiGe:H layer were determined from CPM experiments as $5\times10^{16}\ cm^{-3}$ and 47.6 meV, respectively. The slope of the valence band tail in *a*-Si:H buffer layers and in the *n*-doped layer was adopted as equal to 50 meV. The conduction band tail slope was assumed to be 30 meV in the above two layers and 23 meV in the LBL *a*-SiGe:H layer, while it was freely chosen in all the band gap graded layers to our convenience for fitting purposes.

B. Results

In Figs. 2–4, the measured and simulated cell characteristics of our *a*-SiGe:H $p-i-n$ solar cells are depicted. The dark $J-V$ characteristics, illuminated (AM1.5 light) $J-V$ characteristics, and the SR curves at short circuit conditions under AM1.5 bias light are shown in Figs. 2–4, respectively. As we mentioned above, the optical parameters, band gaps, activation energies, total densities of the dangling bonds, and valence band slopes were provided by experiments. Most of the other electrical parameters were either adopted within the limited range regularly used in the literature or they do not affect our results. Dangling bond cross sections and band offsets are the only little known parameters that affect our simulated $J-V$ and SR curves. However in this article we will discuss general trends that are independent of the values adopted for these parameters.

We can see in Figs. 2–4 that it is possible to fit the $J-V$ and the SR characteristics of the $p-i-n$ structure in the initial state using either the UDM or the DPM approach. Except for the dangling bond densities all the electrical and optical parameters were assumed to be identical in both models. Table I gives the total DB densities used in the UDM model and the most probable energies E_P used in the DPM model. Identical parameters were adopted for the front and back buffer layers (FB and BB). The same applies for each of the front and back band gap graded layers having the same band gap (FGL and BGL). Interestingly, for fitting purposes, the most appropriate energy E_P of the DPM model tends to lie between the peak energies of the single and double occupied D^- Gaussians of the UDM model. It is important to point out the values of the DB used in the fitting with the UDM. Experimental studies show that the density of the DB in good quality *a*-Si:H materials is around $5\times10^{15}\ cm^{-3}$ and in good quality *a*-SiGe:H with optical gaps near 1.55 eV is

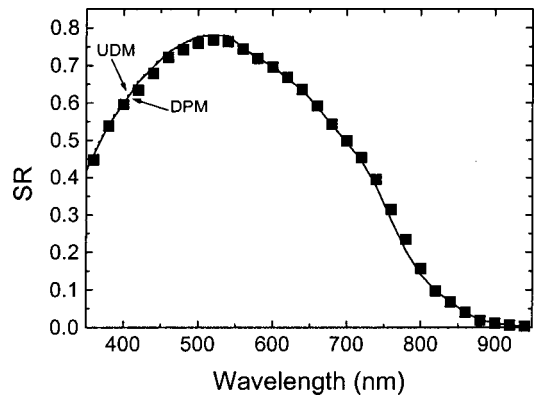

FIG. 4. Measured (square symbols) and simulated spectral response characteristics at short circuit conditions under AM1.5 bias light of the single *a*-SiGe:H $p-i-n$ solar cell. UDM (dotted lines) and DPM (solid lines).

TABLE I. Total DB densities used in the UDM model and most probable dangling bond energies used in the DPM model for fitting purposes. The band gap graded layers (FGLs and BGLs) are shown as 1, 2, 3, and 4 going from buffer layers towards the *i*-*a*-SiGe:H bulk.

Layer	*p*-*a*-SiC:H *n*-*a*-Si:H	FB and BB buffer	FGL and BGL (1)	FGL and BGL (2)	FGL and BGL (3)	FGL and BGL (4)	LBL *i*-*a*-SiGe:H
DB (cm^{-3}) (UDM)	5.0×10^{18} 5.0×10^{18}	2.5×10^{17}	1.75×10^{17}	1.25×10^{17}	9.33×10^{16}	7.0×10^{16}	4.7×10^{16}
D^- (eV) (UDM)	1.30 1.20	1.27	1.24	1.22	1.20	1.16	1.10
E_P (eV) (DPM)	1.30 1.20	1.20	1.17	1.14	1.1	1.05	1.00

around 5×10^{16} cm^{-3}. In a UDM model, the density of the DB of the various layers of the cell should correspond to the density of the DB of individual layers (materials) determined by experiment. In such a case, if we choose a DB density of 5×10^{15} cm^{-3} in our buffer layers and increase this density to 5×10^{16} cm^{-3} going from our buffer layers towards the LBL *a*-SiGe:H layer (as it should be following the properties of the individual layers from the experiments), with D-AMPS we obtain a very optimistic FF (FF$>$0.7) that is quite far from the experimental FF (0.58). However, in order to fit the experimental data, the density of the DB should decrease (in the opposite direction) from doped and buffer layers towards the intrinsic *a*-SiGe:H LBL bulk (as shown Table I). This result gives more support to the defect pool model where the density of DBs increases from bulk to p/i and n/i interfaces.

Figure 5 compares, for the equilibrium state, the density of DBs generated by the defect pool model with the density of DBs used in the uniform density of states model in order to fit the $J-V$ and SR experimental curves. We can clearly see that for the UDM case, in order to make fittings possible, in the LBL, FGL, and BGL layers the density of the DB increases when we move towards the doped layers. Another interesting feature is that the DPM tends to generate more DBs near the p/i interface than near the i/n interface, due to the dependence of the DB with the position of the Fermi level. The comparison of the electric field profiles indicates that the DPM model tends to increase the electric field in the FGL and BGL layers and to lower the electric field inside the LBL layer with respect to the UDM model (see Fig. 6). The DPM model tends to generate more positive trapped charges on the left-hand side of the LBL and in FGL layers and more negative trapped charges on the right-hand side of the LBL layer and in BGL layers than the UDM model. This can be clearly seen in the front region of the device in Fig. 5. In the back region of the device we have to keep in mind that only between 2/5 and 3/7 of the total density of DBs is effective in generating negative charge in the UDM model. Higher trapped charge concentrations near the p/i and n/i interfaces weaken the electric field in the LBL region. Recombination losses are more pronounced in the LBL layer for the DPM model and in the FGL and BGL for the UDM model. We have to keep in mind that in lower band gap materials (like, for instance, in *a*-SiGe:H) midgap states take control of trapping and recombination processes over tail states. The scenario is quite different in *a*-Si:H where tails and midgap states compete with each other to define the total trapped charge and the recombination losses.

C. Computer predictions using the UDM and the DPM models

In order to optimize the performance of the single junction $p-i-n$ *a*-SiGe:H solar cell we studied the dependence of the efficiency with respect to device layer thickness using the input parameters extracted from our fittings. Although we

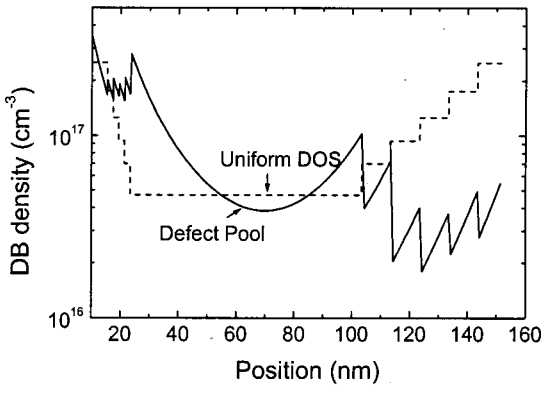

FIG. 5. Comparison of the dangling bond densities generated by the defect pool model (solid line) and those used in the uniform density of states model (dashed line) to fit $J-V$ and quantum efficiency QE experimental curves.

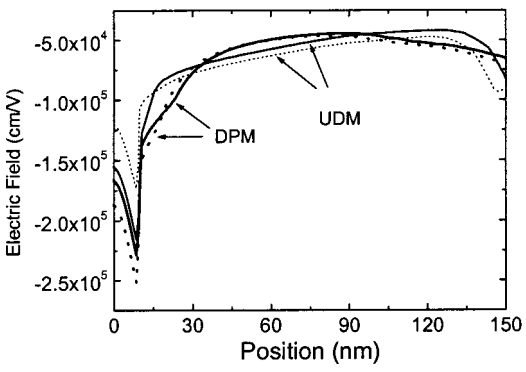

FIG. 6. Change in the electric field profile under short circuit conditions when the front buffer layer is removed. Solid lines correspond to the solar cell with the FB layer and dotted lines correspond to the same solar cell without the buffer layer. The light source is TFAM1.5 red bias light.

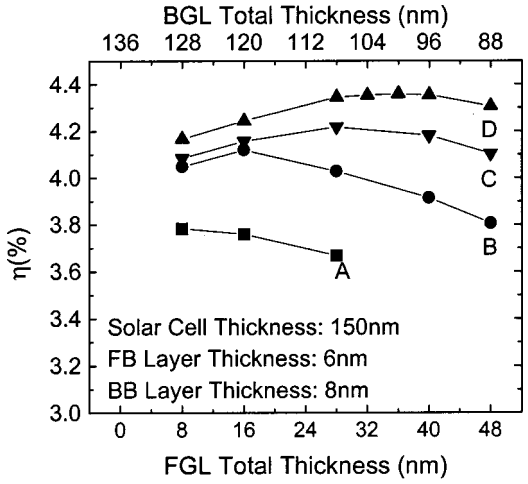

FIG. 7. Dependence of the solar cell efficiency under TFAM1.5 red bias light with respect to the front and back band gap graded layer thicknesses. The density of the dangling bond is modeled with the defect pool model. LBL thickness: (A) 80, (B) 40, (C) 20, (D) 10 nm. (BGL Total thickness =BGL thickness+LBL thickness).

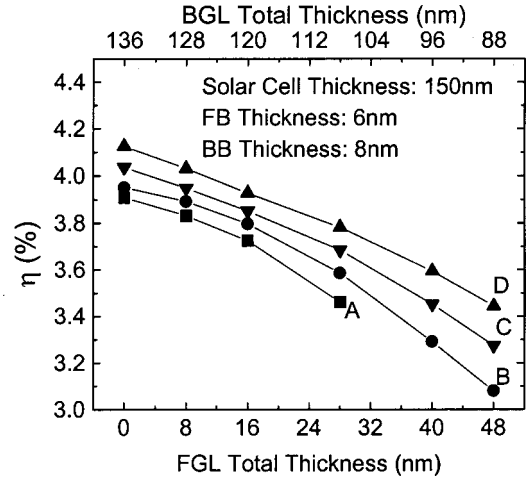

FIG. 8. Dependence of the solar cell efficiency under TFAM1.5 red bias light with respect to the front and back band gap graded layer thicknesses. The density of the dangling bond is modeled with the uniform density of states model. LBL thickness: (A) 80, (B) 40, (C) 20, (D) 10 nm. (BGL Total thickness=BGL thickness+LBL thickness).

were able to reproduce three experimental curves adopting either the UDM or the DPM model, the dependences of the solar cell efficiencies with respect to layer thickness predicted by D-AMPS are entirely different when we choose one model over the other.

As we are specifically interested in the application of *a*-SiGe:H $p-i-n$ structures for use as bottom subcells of *a*-Si:H/*a*-SiGe:H tandem solar cells, we will do our simulations using the light source that results from filtering AM1.5 light through a thin *a*-Si:H layer that has the same thickness as the intrinsic layer used in the top subcell of our *a*-Si:H/*a*-SiGe:H tandem cells. Experimentally these tandem cells showed an efficiency of 9.14%. This light spectrum that results after the absorption of the AM1.5 light by one pass through the *a*-Si:H thin film is termed TFAM1.5 light.

The sample used to fit the bottom of this tandem structure (Figs. 2–4) has a total thickness (excluding both doped layers) of 142 nm. As the first step in optimizing the performance of the single *a*-SiGe:H solar cell, the simulations predict improvement in the annealed state by elongating the back grading. Taking in advance the possible future degradation for too thick samples, we have fixed the total thickness of the *i* layer at 150 nm. This thickness excluded both doped layers and guarantees the presence of a strong enough electic field inside of the intrinsic layer to protect the cell from the Staebler–Wronski (SW) effect. Having decided to fix the total thickness at 150 nm, the second step is gross tuning of the thickness of the layers. We begin by varying all devices layer thickness in an attempt to seek higher efficiencies. By decreasing the LBL thickness (this layer introduces significant recombination losses) and by changing the FGL and BGL layer thicknesses we move from a LBL thickness of 80 nm [curve A, Figs. 7 and 8] to a thickness of 10 nm [curve (D), Figs. 7 and 8]. Figure 7 represents the prediction made using the DPM while Fig. 8 shows the predictions made with the UDM. The four layers that constituted front grading of equal thickness are adopted. The same is applied to the back grading. During gross tuning, we varied the FGL and BGL for every thickness of the LBL (as can be seen in Figs. 7 and 8), keeping the thickness of the buffers unchanged. The DPM predicts improvement of the efficiency with the following thicknesses: FB (6 nm), FGL ($9\times4=36$ nm), LBL (10 nm), BGL ($22.5\times4=90$ nm), and BB (8 nm). With these changes we are able to obtain improvement in our efficiency under TFAM1.5 light from 3.76% (efficiency of our sample) to 4.359%. These new thicknesses define our new baseline solar cell structure. Using the UDM we instead reach the conclusion that FGL layers should be removed (see Fig. 8).

We have chosen the best profile predicted by the DPM and a profile with 16 nm of FGL and 10 nm of LBL from the

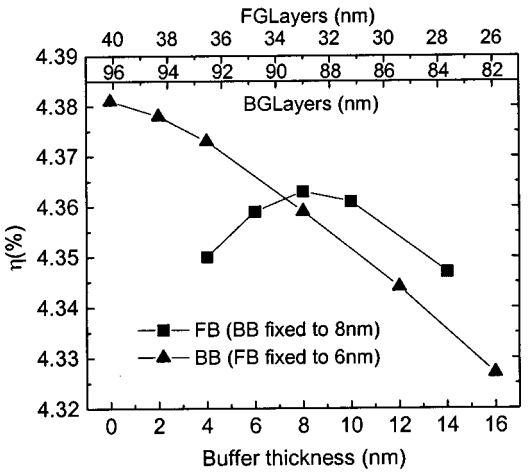

FIG. 9. Dependence of the solar cell efficiency under TFAM1.5 red bias light with respect to the front and back buffer layer thicknesses in the DPM model. The LBL layer thickness is fixed at 10 nm. In the low *x* axis we show the FB (BB) layer thickness and in the top *x* axis we show the total FGL (BGL) layers thickness (both in nm). The FGL (BGL) layers thickness is in one to one correspondence with the FB (BB) layer thickness only (to keep the total thickness constant).

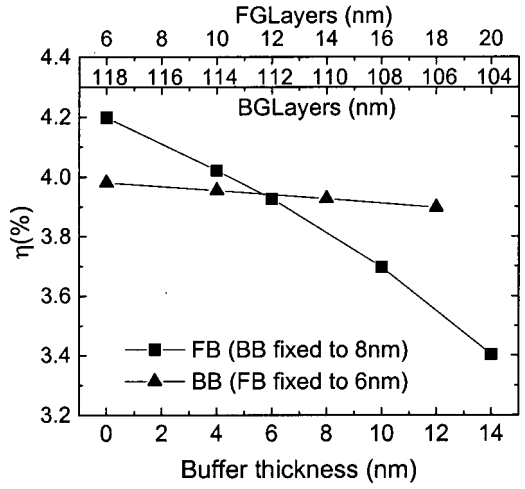

FIG. 10. Dependence of the solar cell efficiency under TFAM1.5 red bias light with respect to the front and back buffer layer thicknesses in the UDM model. The density of the dangling bond is modeled assuming constant values inside each device layer. The LBL layer thickness is fixed at 10 nm. In the low *x* axis we show the FB (BB) layer thickness and in the top *x* axis we show the total FGL (BGL) layers thickness (both in nm). The FGL (BGL) layers thickness is in one to one correspondence with the FB (BB) layer thickness only (to keep the total thickness constant).

prediction of the UDM. With theses two profiles we have performed fine-tuning, changing the thickness of the buffers. In Figs. 9 and 10 we increase (decrease) the FB (BB) layer thickness, decreasing (increasing) simultaneously the FGL (BGL) layer thicknesses and keeping intrinsic layer total thickness (W) constant. In Figs. 9 and 10 the LBL layer thickness was fixed at 10 nm. In the low x axis we have the FB (BB) layer thickness and in the top x axis we have the four layer FGL (BGL) thicknesses added up. Figures 7 and 8 correspond to what we call gross tuning of our solar cell performance and Figs. 9 and 10 correspond to fine-tuning of our efficiency. Let us discuss first the predictions obtained for the front layer FB and FGL.

FB and FGL layers: The first important difference found in our computer predictions is that an optimum thickness for the front buffer layer (FB) is recommended by D-AMPS when the DPM model is invoked but entire removal of the FB layer is advised by D-AMPS when the UDM model is implemented. Another striking difference between the predictions of our code for these two different DB representations is that an optimum thickness is found for the front band gap graded layers within the DPM model but the highest efficiency is achieved when these four FGLs are removed in the UDM model. Both predictions of D-AMPS when the UDM is used are in contrast with experimental experience, while those of D-AMPS when the DPM model is used are in agreement with experimental practice. In order to understand the origin of such different predictions we inspected the computer generated electric field, trapped carrier concentration, and recombination rate profiles.

UDM model: It is known that the presence of front layers (FBs or FGLs) introduces redistribution of the electric field in the solar cell. The positive charge trapped in these layers (D^+ states predominates) enhances the electric field around the p/i interface and weakens the electric field in the intrinsic layer's bulk. In the UDM approach, when the FB or FGL layers are made thinner or when they are directly removed, the electric field becomes reinforced in the intrinsic *i*-*a*-SiGe:H bulk where recombination losses are more significant due to the lower mobility gap and the higher density of DBs present in the LBL layer. At the same time the electric field is weakened at the front region of the *i*-*a*-SiGe:H layer near the p/i interface where recombination losses are less important (see Fig. 6). This redistribution of the electric field when FBs of FGLs are removed produces a net reduction of the global recombination loss present in the solar cell and gives rise to improvement of its overall performance (see Fig. 10).

DPM model: In Fig. 5 we can see that the DPM model introduces a significant density of DBs at the left-hand side of the LBL *i*-*a*-SiGe:H layer. These dangling bonds are mostly D^+ states and provide positive trapped charge. Similarly DBs introduced by the DPM model at the right-hand side of the LBL *i*-*a*-SiGe:H layer are mostly D^- states and provide negative trapped charge. These extra D^+ and D^- states generated by the DPM tailor in a significant proportion the electric field profile inside the LBL layer. Hence, when the FBs or FGLs are made thinner or are removed, the electric field in the intrinsic layer bulk is much less affected in the DPM model than in the UDM model. The DB profile generated by the DPM model inside the LBL layer already defines the electric field profile to a great extent. The second important point is that when the DPM model is invoked the removal of front layers in the *a*-SiGe:H single junction $p-i-n$ solar cells still produces a redistribution on the electric field that is quite different to the one found in the UDM model. When front layers are made thinner or are removed the Fermi level in equilibrium moves closer to the valence band edge in the front region of the intrinsic layer which forces the DPM model to generate a higher concentration of D^+ states near the p/i interface. These additional D^+ states reinforce the electric field over the FB and over the FGL layers and in the back region of the LBL layer and weaken the electric field over the front part of the LBL region (see Fig. 6). This redistribution of the electric field is quite different to the one observed in the UDM model. The third point to make is that these additional D^+ states created by the DPM model not only strengthen the electric field but also increase recombination losses near the p/i interface. This trend is never observed in the UDM model where an increase (decrease) of the electric field is usually accompanied by a decrease (increase) of recombination losses. As a result of this there is a trade-off between too thin and too thick FB or FGL layers. Very thin FB or FGL layers have the negative effect of weakening the electric fields in the front region of the LBL layer where DBs are mainly D^+ states and recombination losses are significant. Very thick FB or FGL layers have the negative effect of weakening the electric field in the back region of the LBL layer where DBs are mainly D^- states and recombination losses are also important (Figs. 7 and 9). In the UDM model the physics are simpler: Thinner FB or FGL layers just enhance the electric field in the entire LBL region, decreasing the overall recombination losses, and

thicker FBs or FGLs produce the opposite effect.

BB and BGL layers (UDM and DPM models): When BB or BGL layers are made thinner we also observe redistribution of the electrical field in the intrinsic *a*-SiGe:H layer. In UDM model the electrical field becomes weaker at the back region and stronger at the front region of the intrinsic layer. Hence recombination losses become stronger and weaker at the back and at the front sides of the intrinsic region, respectively. The most significant changes in recombination losses take place in the back region of the intrinsic layer which makes D-AMPS predict higher efficiencies for thicker BGLs (see Fig. 8). In the DPM model the field becomes stronger at the back region of the intrinsic layer and weaker at the front region of the intrinsic layer. However recombination losses also increase in the back region of the intrinsic layer for thinner BB or BGL layers. The Fermi level in equilibrium is placed closer to the conduction band edge in the back region of the intrinsic layer which forces the DPM model to generate more DBs (D^- states), enhancing simultaneously the electric field and the recombination losses. As a result of this, both models predict similar trends but different thicknesses for the BGL layers, as can be seen in Figs. 7 and 8.

The solar cell efficiency is more sensitive to changes in thickness performed on front layers than on the back layers. The boundary condition of keeping the total solar cell thickness W constant conditions our results. It is important to notice that both the UDM and the DPM models suggest the removal of the BB layer. However we have to keep in mind that when the BB layer is made thinner the BGL layers are at the same time becoming thicker which results in better optical absorption. By using the DPM model for our efficiency fine-tuning we were able to improve the efficiency of our baseline case, first, from 4.359% to 4.363% by redefining the FB thickness to 8 nm and, second, to 4.381% by removing the BB layer (see Fig. 9). In our baseline case we were already very near the maximum efficiency (the total thickness is kept equal to 150 nm).

We also studied the dependence of the efficiency of the *a*-SiGe:H $p-i-n$ solar cell with respect to each layer thickness under AM1.5 bias light. Although different optimum layer thicknesses were obtained for these two light sources similar trends were predicted by D-AMPS under either AM1.5 or TFAM1.5 illumination.

We also made simulations changing, one by one, the buffer, the band gap graded and the low band gap layer thickness but without keeping the total solar cell thickness W equal to 150 nm. We found that when we use the UDM model D-AMPS predicts the highest efficiency for the entire removal of FB, BB, and FGL layers. On the other hand, when we use the DPM model D-AMPS predicts optimum thicknesses of 6 nm for the FB layer, 4 nm for each FGL layer, 10 nm for the LBL layer, 40 nm for each BGL layer, and 12 nm for the BB layer. For this configuration the efficiency achieved under TFAM1.5 illumination is 4.59% and the total thickness is 204 nm.

Summarizing, we can say that using the uniform density of state model we cannot justify with D-AMPS the implementation of U- or V-shape band gap profiles in the intrinsic layer of single junction $p-i-n$ *a*-SiGe:H solar cells to improve its performance. On the contrary, using the defect pool model in our computer simulations we are able to demonstrate the benefits of U-shape band gap profiles for the intrinsic *a*-SiGe:H layer, in agreement with the experimental work of Guha *et al.*[1,2]

D. Behind higher efficiencies

Having learned that the DPM is appropriate to generate realistic computer predictions, in agreement with observed experimental trends, we investigate the possibility of increasing the initial efficiency of our *a*-SiGe:H $p-i-n$ solar cell by varying the different layer thicknesses of our device but keeping the total thickness W equal to 150 nm. We studied with D-AMPS the single *a*-SiGe:H $p-i-n$ solar cells under TFAM1.5 illumination. The LBL layer was fixed at 10 nm in order to maximize the solar cell efficiency (see Figs. 7 and 8). In both structures we found that the solar cell performance can be improved by adopting nonequal thicknesses for the four FGL and BGL band gap graded layers. Our simulations indicate that it is more convenient to deposit thicker FGL and BGL layers near the LBL layer and thinner layers near the buffer layers. The increase of FGL and BGL layer thicknesses near the LBL layer enhances the optical generation of free carriers inside the intrinsic layer and slightly reinforces the electric field within band gap graded layers. This alternative design for the *a*-SiGe:H intrinsic layer significantly enhances J_{sc} and introduces minor changes in the FF and V_{oc} in both the single junction $p-i-n$ structure and in the tandem solar cell. We observed a relative improvement of solar cell efficiency higher than 4%. It is important to say that equal thicknesses for all the FGL and BGL layers is synonymous to band gap linear grading because in each step of our FGL and BGL layers the mobility band gap was reduced by equal amounts. Our predictions imply that other band gap profile shapes, different from the U or V shape or linear band gap grading, are more appropriate for better performance. This optimum band gap shape seems to be either exponential or parabolic and we are currently investigating its analytical expression. Our initial *a*-SiGe:H $p-i-n$ solar cells deposited with band gap graded layers of nonequal thicknesses have confirmed these simulation predictions.

IV. CONCLUSIONS

We studied the single junction *a*-SiGe:H $p-i-n$ solar cell in the initial state with computer simulations. We were able to fit the dark and the illuminated current voltage characteristics and the spectral response curve under short circuit conditions. These fittings were performed using either a uniform density of states in each layer or the defect pool model. When we model each layer of *a*-SiGe:H $p-i-n$ solar cells with a uniform density of states we are not able to justify the advantages of introducing a U-shaped band gap profile into the *a*-SiGe:H intrinsic layer. On the other hand, by implementing the defect pool model in our computer code we are able to predict an optimum thickness for the front buffer layer and for the front band gap graded layers. We conclude that to properly design the band gap profile in *a*-SiGe:H solar

cells in particular and to appropriately model *a*-Si:H based solar cells in general it is necessary to include the defect poolmodel in the computer simulations. Using the defect pool model we predict higher efficiencies for the single junction *a*-SiGe:H $p-i-n$ solar cell when the staircase band gap profile in the intrinsic layer is implemented with thicker steps besides the lowest band gap *a*-SiGe:H layer and thinner steps besides the p/i and i/n interfaces.

ACKNOWLEDGMENTS

The authors highly appreciate the financial support of The Netherlands Organization for Energy and Environment (NOVEM) and of the Agencia Nacional de Promoción Cinetfica y Technológica, Project No. 10-00000-0095. They thank Karine van der Werf for depositions and for preparation of the solar cell samples.

[1] S. Guha, J. S. Payson, S. C. Agarwal, and S. R. Ovshinsky, J. Non-Cryst. Solids **97&98**, 1455 (1987).
[2] S. Guha, J. Yang, A. Pawlikiewicz, T. Glatfelter, R. Ross, and S. R. Ovshinsky, Appl. Phys. Lett. **54**, 2330 (1989).
[3] J. Zimmer, H. Stiebig, and H. Wagner, J. Appl. Phys. **84**, 611 (1998).
[4] J. Zimmer, T. Brammer, D. Lundszien, H. Stiebig, R. Carius, and H. Wagner, Proceedings of the 16th European Photovoltaic Solar Energy Conference and Exhibition, Glasgow, Scotland, 2000, p. 381.
[5] P. J. McElheny, J. K. Arch, H. S. Lin, and S. J. Fonash, J. Appl. Phys. **64**, 1254 (1988).
[6] H. Okamoto, H. Kida, and Y. Hamakawa, Philos. Mag. B **49**, 231 (1984).
[7] M. J. Powell and S. C. Deane, Phys. Rev. B **48**, 10815 (1993).
[8] M. J. Powell and S. C. Deane, Phys. Rev. B **53**, 10121 (1996).
[9] F. A. Rubinelli, J. D. Ouwens, and R. E. I. Schropp, Proceedings of the 13th European Photovoltaic Solar Energy Conference and Exhibition, Nice, France, 1995, p. 195.
[10] F. A. Rubinelli and R. E. I. Schropp, Proceedings of the 2nd World Conference on Photovoltaic Solar Energy Conference, Vienna, Austria, 1998, p. 998.